Unconventional optical response in monolayer graphene due to dominant intraband scattering

Palash Saha and Bala Murali Krishna Mariserla*
Ultrafast Physics Group, Department of Physics, Indian Institute of Technology Jodhpur, Rajasthan 342037, India

(Received 11 September 2023; revised 8 March 2024; accepted 12 March 2024; published 25 March 2024)

Scattering dynamics influences the graphene's transport properties and inhibits the charge carrier deterministic behavior. The intra/interband scattering mechanisms are vital for graphene's optical conductivity response under specific considerations of doping. In this study, we systematically explored the impact of scattering on optical conductivity using a semiclassical multiband Boltzmann equation, incorporating both electron-electron and electron-phonon interactions collectively with a single phenomenological relaxation time constant. We found unconventional characteristics of linear optical response with a significant deviation from the universal conductivity ($e^2/4\hbar$) in doped monolayer graphene. This is explained through phenomenological relaxation rates under low doping regime with dominant intraband scattering. Such novel optical responses vanish at high temperatures or overdoping conditions due to strong Drude behavior. With the aid of approximations around Dirac points we have developed analytical formalism for many-body interactions and are in good agreement with the Kubo approaches.

DOI: 10.1103/PhysRevB.109.125428

I. INTRODUCTION

Unique and remarkable quantum properties of monolayer graphene with a honeycomb structure have sparked significant interest in both linear [1] and nonlinear optics [2]. The Dirac cone symmetry is responsible for the ambipolar behavior thus producing a surge of carrier concentration in suspended graphene [3,4] and encapsulated graphene [5]. This is in contrast to the semiconductors where a particular quasiparticle plays a major role for the transport properties [6]. The charge carriers in graphene with zero rest mass resembles the relativistic entities and exhibit an effective velocity comparable to the speed of light [7,8]. These distinctive characteristics of charge carriers in pristine graphene are at the helm of its high conductivity [9,10]. In order to describe the electronic properties of different two-dimensional materials, the tight-binding Hamiltonian is a first simplified noninteracting model and commonly used on monolayer, bilayer, and twisted graphene [11–13]. This basic model reveals the behavior of π electrons in the graphene hexagonal lattice by considering the interaction between neighboring carbon atoms through electron hopping and overlapping of their atomic orbitals, which successfully produces the electronic band structure including linear dispersion near Dirac points. To calculate the optical conductivity of graphene using the tight-binding Hamiltonian, one can employ the Kubo expression [14–16] from the linear response theory [17]. But the current-current correlation function in the Kubo expression requires summation over all the states in high-dimensional systems, which can become computationally expensive.

Besides the Kubo approach, the semiconductor Bloch equation (SBE) [17,18] is an alternative and more effective to calculate the optical conductivity of semiconductors and two-dimensional crystals. The SBE is derived from the time-dependent Schrödinger equation for periodic systems that provides great advantage in solving the out-of-equilibrium problems. Within the realm of this SBE, a cascade of different studies has been focused to observe a spectrum of diverse optical phenomena. Out of which, Cheng, Sipe, and Vermuelen conducted extensive study on doped monolayer graphene to obtain linear and nonlinear optical conductivity with scattering [19] and without scattering [20] using approximations around Dirac points. With the similar assumptions, they have calculated dc current-induced second harmonic generation [21] at zero temperature limit. A quite similar research has been conducted by Hipolito, Taghizadeh, Alireza, and Pedersen [22] to find the linear conductivity, third harmonic generation, and optical Kerr effect for both monolayer and bilayer graphene. Identification of new kinds of third-order divergences during cross phase modulation and degenerate four wave mixing were carried out by Cheng, Sipe, Wu, and Guo [23] for centrosymmetric two-dimensional materials. Naib and Sipe [24] detected intraband and interband current with applying electric field through numerical simulation on undoped monolayer graphene at low temperatures. McGouran *et al.* [25] obtained dipole matrix elements through length gauge and found the linear and nonlinear Terahertz responses for undoped suspended bilayer graphene through numerical simulations at different low temperatures with scattering time of 80 fs. Study of carrier mobility, carrier density, band structure, linear and nonlinear terahertz response of nitrogen doped graphene were reported [26] using this technique. Cheng and Guo [27] studied the nonlinear magnetooptic effects in doped and gapped graphene and examined linear response, third harmonic generation, Kerr effects, two photon absorption, and four wave mixing under external magnetic field ($B = 0.05$ T). The previous studies were using nonlinear relaxation rates

*bmkrishna@iitj.ac.in

for studying higher-order optical phenomenon and less focus on the influence of equal rates for different orders, which should be exercised to understand anomalous linear optical responses.

In this paper, the linear optical response for monolayer graphene is investigated using the SBE approach with the many-particle approximations at different doping levels. Theoretically, the length gauge approach for the equation of motion with the density matrix has been used innumerable times to investigate various optical parameters. The different scattering mechanisms are introduced in our calculations with the aid of phenomenological relaxation parameters to the modified SBE and the conductivity response is obtained from the first-order density matrix, which comprises of both intra- and interband components. Furthermore, the results are compared with experimental results to gain more insights about the Pauli blocking and conductivity response. Our formalism is in good agreement with the experimental data with slight deviations due to the approximations near Dirac points, lower optical field energy and noninclusion of thermal fluctuations. We have shown that the utilization of approximations around Dirac points bridge the results obtained from perturbative calculations and the Kubo expression under an external electric field.

II. SEMICLASSICAL APPROACH

The SBE consists of perturbed Hamiltonian with radiation-interaction and scattering terms to study many-body interactions. For the graphene, unperturbed tight-binding Hamiltonian ($\hat{H}_0$) deals with the nearest-neighbor hopping with zero on-site energies,

$$\hat{H}_0 = \sum_n \sum_k \varepsilon_{nk} c^{\dagger}_{nk} c_{nk}. \tag{1}$$

The energy eigenvalues are denoted by ε_{nk} and the coefficients $c^{\dagger}$, c are creation and annihilation operators with states $n = [1, 2]$ in the momentum space (k). Previously, the light-matter interactions were treated with velocity gauge, but challenges arise for many-body interactions because of the spurious divergences at lower frequencies due to its sensitivity and susceptibility to numerical inaccuracies [28]. These divergence issues can be easily tackled by using the length gauge through sum rules [29] and gauge invariant electric field, which emerged as a pivotal solution to the problem. However, it does possess an additional scalar dependence that disturbs the diagonal property of the perturbed Hamiltonian in k space. Because of that, there will be some overlap or coupling contributions, which can be eliminated by the band isolation technique [30].

The light-matter interacting term in the Hamiltonian ($\hat{H}_{eR}$) possesses interaction between electric field of the light and charge distribution of the matter. By considering electric dipole approximation along with long wavelength limit for uniform illumination, we have employed the length gauge approach with explicit dependence on external electric field $\boldsymbol{E}$(t) given by,

$$\hat{H}_{eR} = -e\mathbf{E}(t).\hat{\mathbf{r}}, \tag{2}$$

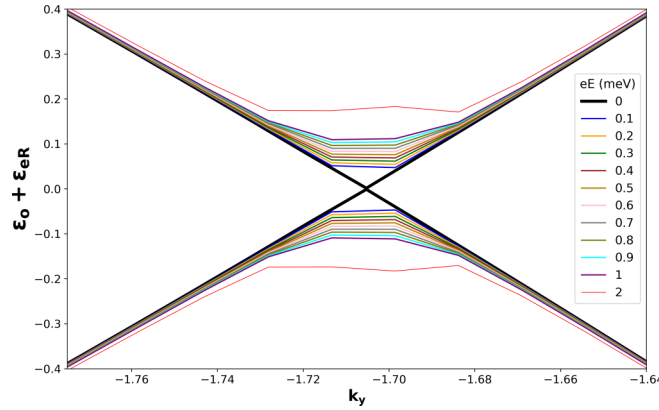

FIG. 1. Incorporation of light-matter interaction energy (ε_{eR}) into the tight-binding component (ε_o) with hopping parameter ($t = -2.7$ eV) introduces a more significant band gap expansion, even at relatively low electrical bias (eE).

where e is the charge of the electron and $\hat{\boldsymbol{r}}$ being the spatial coordinates. The position operator in the length gauge approach is linked to the Berry connection (ξ) when the bands are distinct under external electrical field. In the context of distinct bands, the Berry connection or Berry curvature may capture the geometric phase relationship between them when system undergoes adiabatic changes in parametric space. Close proximity of the Dirac cones (Fig. 1) is no longer valid due to presence of external electric field radiation within the light-matter Hamiltonian [19] given by,

$$\hat{H}_{eR} = -e\mathbf{E}(t). \sum_{n_1} \sum_{n_2} \sum_k c^{\dagger}_{n_1 k} \boldsymbol{\xi}_{n_1 n_2 k} c_{n_2 k} - ie\mathbf{E}(t). \sum_n \sum_k \nabla_k c^{\dagger}_{nk} c_{nk} \tag{3}$$

in which the last term possesses local band characteristics. The effect of electron-electron, electron scattering due to phonon, and impurities are dealt with by scattering term in the Hamiltonian. In the equation of motion [Eq. (4)], the rate of change due to scattering can be made proportional to the density of states with the inclusion of phenomenological relaxation parameter.

A. Collisional multiband Boltzmann equation

We have adopted Sipe-Aversa's SBE [30] with length gauge perturbation theory to develop the equation of motion and solved for the response function of monolayer graphene. In general, most of the calculations are always focused on interband scattering contribution while neglecting the intraband scattering. Using a modified SBE, we take intraband information directly into account with the aid of phenomenological relaxation parameters. To obtain expression for many-body interactions, we followed semiclassical approach using the quantum Liouville equation,

$$i\hbar \frac{\partial \hat{\rho}(t)}{\partial t} = [\hat{H}, \hat{\rho}(t)], \tag{4}$$

which consists of the total Hamiltonian ($\hat{H}$) and the time-dependent density operator denoted by,

$$\hat{\rho}(t) = \sum_{n_1 n_2} \rho_{n_1 n_2}(t)|n_1\rangle\langle n_2|, \tag{5}$$

where, $\hbar$ is the reduced Planck's constant. Using Eqs. (4) and (5) the equation of motion in terms of density matrix is obtained,

$$\begin{aligned} i\hbar\frac{\partial \rho_{n_1 n_2}(t)}{\partial t}|n_1\rangle\langle n_2| = \hat{H}_0|n_1\rangle\rho_{n_1 n_2}(t)\langle n_2| - \rho_{n_1 n_2}(t)|n_1\rangle\langle n_2|\hat{H}_0 \\ - i\Gamma_{n_1 n_2}\rho_{n_1 n_2}(t)|n_1\rangle\langle n_2| \\ - e\mathbf{E}(t).\langle n_1|[\hat{\mathbf{r}}, \hat{\rho}(t)]|n_2\rangle|n_1\rangle\langle n_2|, \end{aligned} \tag{6}$$

where Γ is the phenomenological constant, which contains the scattering parameters. In the presence of the scattering, the time evolution of the density operator undergo various physical effects including damping or decoherence. We have used the band isolation identity [30] to get a commutation relationship for the spatial coordinate ($\hat{\mathbf{r}}$) with a physical operator($\hat{\Lambda}$),

$$\begin{aligned} \int dr \Psi^*_{n_1 k_1}(r)[\hat{\mathbf{r}}, \hat{\Lambda}]\Psi_{n_2 k_2}(r) \\ = \left[\boldsymbol{\xi}_{k_1 k_2}, \Lambda_{k_1 k_2}\right]_{n_1, n_2} + i\nabla_k \Lambda_{n_1 n_2 k_1 k_2}. \end{aligned} \tag{7}$$

In general, the single-band Boltzmann equation can model the charge carrier transport in a single electronic band, which can be extended for the multiband. To depict these different band characteristics, the above Eq. (7) is extended for each k values to perceive the required collisional multiband Boltzmann equation (CMBE),

$$\begin{aligned} i\hbar\frac{\partial \rho_{n_1 n_2 k}(t)}{\partial t} = \left(\varepsilon_{n_1 k} - \varepsilon_{n_2 k}\right)\rho_{n_1 n_2 k}(t) - ie\mathbf{E}(t).\nabla_k \rho_{n_1 n_2 k}(t) \\ - e\mathbf{E}(t).\sum_n \left(\boldsymbol{\xi}_{n_1 n k}\rho_{n n_2 k}(t) \right. \\ \left. - \rho_{n_1 n k}(t)\boldsymbol{\xi}_{n n_2 k}\right) - i\Gamma_{n_1 n_2 k}\rho_{n_1 n_2 k}(t). \end{aligned} \tag{8}$$

The right-hand side of this equation of motion is equivalent in form to the quantum Boltzmann equation (QBE). It consists of the kinetic energy terms, which seem to combine with the dot product of scalar potential. Eliminating the reliance of this offset energy on position and maintaining system uniformity, the mentioned identity offers an alternative advantage. And, finally the extra driving term collectively accounts for all the collisions, which is the identical term from QBE.

B. Conductivity expression

Composition of the jth order CMBE is possible if the density matrix is considered to be sum of all orders,

$$\begin{aligned} \hbar\frac{\partial \rho^{(j)}_{n_1 n_2 k}(t)}{\partial t} = -i\left(\varepsilon_{n_1 k} - \varepsilon_{n_2 k}\right)\rho^{(j)}_{n_1 n_2 k}(t) - \Gamma^{(j)}_{n_1 n_2 k}\rho^{(j)}_{n_1 n_2 k}(t) \\ + ie\mathbf{E}(t).\left[\boldsymbol{\xi}_k, \rho^{(j-1)}_k(t)\right]_{n_1 n_2} \\ - e\mathbf{E}(t).\nabla_k \rho^{(j-1)}_{n_1 n_2 k}(t). \end{aligned} \tag{9}$$

The solution of the CMBE equation is in the following form,

$$\rho^{(j)}_{n_1 n_2 k} = \int .. \int \left[-e\frac{d\omega}{2\pi}E^a_\omega e^{-i\omega t}\right]^j \mathcal{S}^{(j)}_{n_1 n_2 k}(\omega_1, \omega_2, \ldots, \omega_j), \tag{10}$$

where, $\mathcal{S}(\omega)$ is the jth-order frequency component. By making use of the perturbative expansion of the current density, a pathway opens for establishing a connection with the surface current density given by,

$$\begin{aligned} e\sum_{n_1 n_2}\int \frac{d\mathbf{k}}{4\pi^2} v^a_{n_1 n_2 k}\rho^{(j)}_{n_1 n_2 k}(t) \\ = \int .. \int \left[\frac{d\omega}{2\pi}E^a_\omega e^{-i\omega t}\right]^j \sigma^{(j);abcd..}(\omega_1, \omega_2, \ldots, \omega_j). \end{aligned} \tag{11}$$

After substitution of Eq. (10) in Eq. (11), we get the generalized formula for conductivity,

$$\sigma^{(j);abcd..} = -e^{j+1}\sum_{n_1 n_2}\int \frac{d\mathbf{k}}{4\pi^2} v^a_{n_1 n_2 k}\mathcal{S}^{(j);bcd..}_{n_1 n_2 k}(\omega_1, \omega_2, \ldots, \omega_j). \tag{12}$$

Solving the above equation (see Appendix) produces the final expression, which depends upon frequency and chemical potential (μ) given by,

$$\sigma^{(1)xx}_{\text{intra}}(\omega) = \frac{i\sigma_0}{\pi}\frac{4|\mu|}{\hbar\omega + i\Gamma^{(1)}_i} \tag{13}$$

and,

$$\begin{aligned} \sigma^{(1)xx}_{\text{inter}}(\omega) = -\frac{\sigma_0}{\pi}\left[-\pi + iln\left|\frac{\hbar\omega + 2\mu + i\Gamma^{(1)}_e}{\hbar\omega - 2\mu + i\Gamma^{(1)}_e}\right| \right. \\ \left. + \frac{1}{2}ln\left|\frac{\hbar\omega + 2\mu + \Gamma^{(1)}_e}{\hbar\omega - 2\mu + \Gamma^{(1)}_e}\right|\right], \end{aligned} \tag{14}$$

where, Γ_e is the interband constant, Γ_i is the intraband constant, and $\sigma_0 = (e^2/4\hbar)$ is the universal conductivity. In the case of graphene, the Dirac cone electronic dispersion leads to a unique Drude response and the expression of Drude conductivity for Dirac electrons is the intraband conductivity in Eq. (13), which coincides with the Boltzmann-Drude expression. In connection to this, direct gap approximation is needed to be considered when the Berry connection is dealing with interband transition. It is well assumed that the momentum states in both bands ($|ck\rangle$ for CB and $|vk\rangle$ for VB) has to be aligned ($\Delta k = 0$), thus restricting the oblique transitions. Not only for Berry connection, this approximation is true to any light-matter coupling operator (h') whose matrix element is defined as,

$$\langle ck|\hat{h}'|vk\rangle = \int dr \Psi^*_{ck}(r)\hat{h}'\Psi_{vk}(r) \tag{15}$$

whose Bloch functions are denoted by ψ.

III. RESULTS

In order to explore the linear optical conductivity of the graphene, we use the expressions [Eqs. (13) and (14)] to examine the real and imaginary parts of the optical conductivity

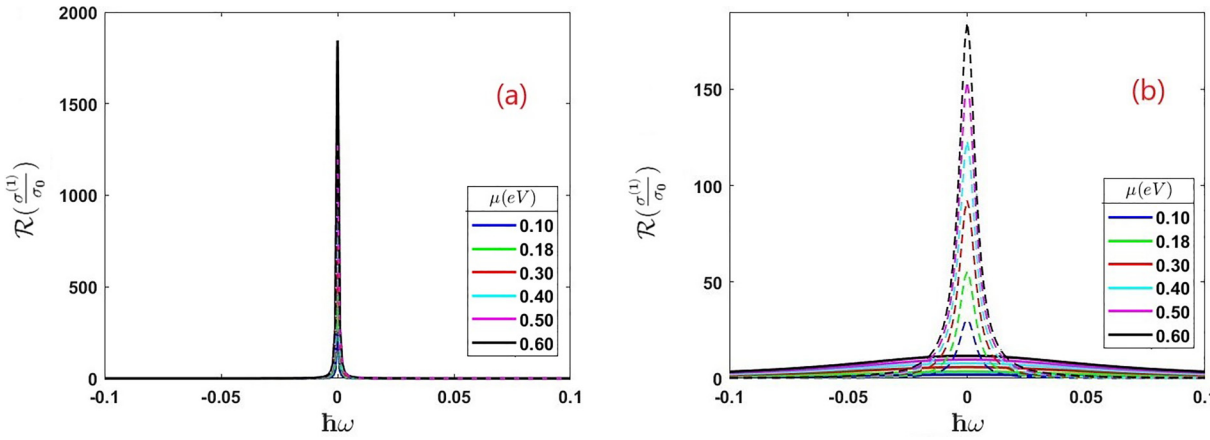

FIG. 2. The solid and dashed lines represent real conductivity of chemical potential values from 0.1–0.6 eV for different scattering rates. (a) Dominant interband scattering induces a narrow width and sharp Drude response [Eq. (13)] near zero frequency. Both solid ($\Gamma_i = 0.5$ meV, $\Gamma_e = 65$ meV) and dashed lines ($\Gamma_i = 0.414$ meV, $\Gamma_e = 4.14$ meV) are overlapped in this case. (b) Dominant intraband scattering reduces the Drude response and increases the broadening for solid lines ($\Gamma_e = 0.5$ meV, $\Gamma_i = 65$ meV) and dashed lines ($\Gamma_e = 0.414$ meV, $\Gamma_i = 4.14$ meV). Γ_i and Γ_e are intraband and interband scattering rates.

with scattering parameters as well as doping levels. The real component of the linear response term, without considering scattering or thermal effects, consists only of the interband contribution as a simple step function, showing optical shielding behavior consistent with the reported literature [20]. The optical conductivity with sole consideration of interband scattering results in reducing the Drude response and a departure from metallic behavior.In our case, with the inclusion of finite scattering, the band terms are expressed independently for transport mechanism. The scattering rates are taken from experimental findings, $\Gamma_e = 4.14$ meV, $\Gamma_i = 0.414$ meV [31], and $\Gamma_e = 0.5$ meV, $\Gamma_i = 65$ meV [32], and employed for a systematic investigation of multiband collisional events while tuning the chemical potential. When we consider intraband scattering, the emergence of new optical response is observed. In the graphene system the interband transitions and associated scattering parameters cannot be avoided, as they play a major role in transport properties. A vital observation from Fig. 2 is showcased in terms of Drude response for different values of chemical potentials and scattering rates. During interband scattering dominance a strong Drude response occurs as shown in Fig. 2(a), is a general case for large availability of free charge carriers. Whereas in the Fig. 2(b), it is strikingly evident that the intraband scattering emerges as a new phenomena, which suppresses the strong free carrier response as well as increasing the bandwidth. Through the variation of the chemical potential, the intensity of Drude behavior is modulated, driven by the interplay between interband and intraband scattering mechanisms. Further, we examine the real conductivity response in the broad infrared frequency range where Pauli blocking (PB) window starts to appear for different scattering rates under the influence of doping. Figure 3(a) is demonstrated with respect to PB effect and found to be more effective with the reduction of interband scattering rate ($\Gamma_e = 10\Gamma_i$) where the slope of the PB curves has sharp cutoff. With higher scattering rates ($\Gamma_e = 130\Gamma_i$) the PB curves slope decreases because of radiation leakage or interband losses, similar behavior is reported by Hipolito *et al.* [22].

When we reverse the scattering dominance process to intraband, we observed that the Drude behavior is suppressed and found emergence of new conductivity peaks at the end of the PB region, which is illustrated in Fig. 3(c). It is evident that the conductivity goes higher than universal conductivity value owing to the prevailing influence of intraband scattering with $\Gamma_e = 0.5$ meV and $\Gamma_i = 65$ meV. This feature is consistent for different doping values but the peak amplitude decreases exponentially with increasing doping concentration. Aforementioned unique feature emerges beyond a specific doping threshold value due to the opening of bandgap, facilitating bound charge carriers, while below this value the dominance shifts to the free carrier Drude response. The higher intraband scattering dominance in our case is closely matching with the experimental results obtained by Basov *et al.* [33] at specific external bias conditions. These experiments were conducted at 28 V gate bias voltage (Fermi level at 0.18 eV) at 45 K, in which the PB curve is bending in the conductivity plot from 0.223–0.447 eV. Whereas in our case, calculations have produced a sharp change in response at 0.367 eV (line **A**) at zero Kelvin, which is lying in region where the slope reaches the maximum as depicted in Fig. 3(c). These electrically neutral quasiparticles participate in band renormalization and compete with the PB mechanism to produce such unique optical responses during weak Coulomb screening. The imaginary part of the conductivity for different scattering rates and doping levels are plotted in Figs. 3(b) and 3(d). The absorption peaks are logarithmic divergences around PB in the conductivity curves. These peak height increases with doping and amplitude get quenched for a high scattering rates. For direct band gap of two-dimensional materials, the energy levels of carriers are shifted due to the interactions between electrons and impurities and enhances the absorption rates at higher doping levels. With the variation of chemical potential one can effectively modulate the absorption to desired frequencies. From Fig. 3(d), the peak at 0.2 eV correspond to midinfrared range is smoothly shifted to near-infrared range with small increment of chemical potential. For a higher interband scattering ($\Gamma_e = 130\Gamma_i$) the broadening of absorption peak

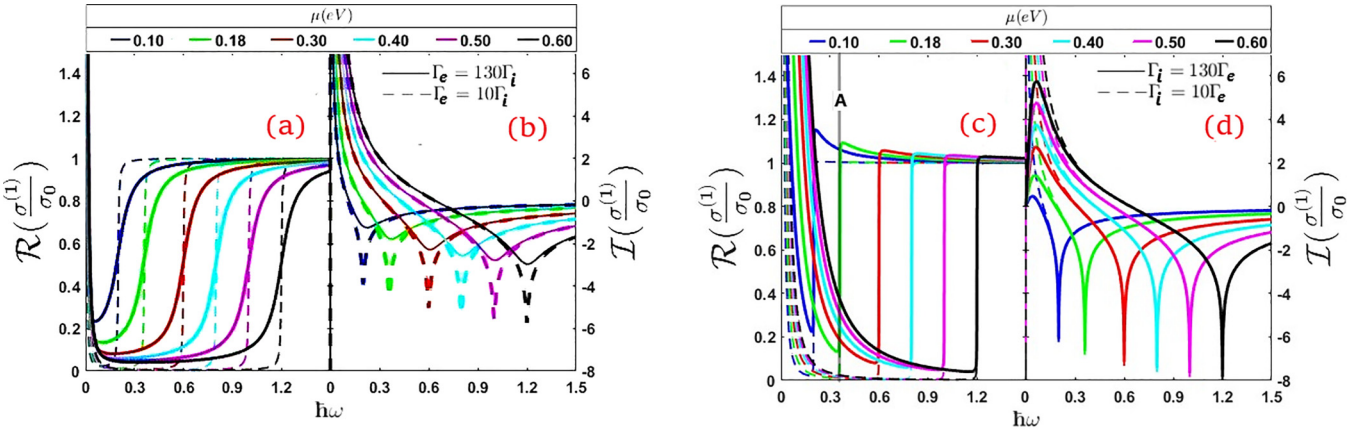

FIG. 3. Both solid and dashed lines represents varying doping levels ranging from 0.1–0.6 eV. The (a) real and (b) imaginary linear conductivity diagrams induced by dominant interband scattering rate has solid lines corresponding to $\Gamma_e = 65$ meV and $\Gamma_i = 0.5$ meV with the dashed lines corresponding to $\Gamma_e = 4.14$ meV and $\Gamma_i = 0.414$ meV, whereas the (c) real and (d) imaginary linear conductivity diagrams induced by dominant intraband scattering rate has solid lines corresponding to $\Gamma_e = 0.5$ meV and $\Gamma_i = 65$ meV with the dashed lines corresponding to $\Gamma_e = 0.414$ meV and $\Gamma_i = 4.14$ meV.

occurs. The smearing in the real part and the broadening in the imaginary part primarily stems from the incorporation of thermal effects, which are inherently considered within our calculations.

IV. CONCLUSION

We have conducted a systematic analytical study on linear optical properties of monolayer graphene under low doping conditions to determine the interplay between interband and intraband scattering mechanisms. A collisional multiband Boltzmann equation was constructed using the length gauge over the velocity gauge to account for many-body effects. The Drude behavior can be tuned through the phenomenological scattering parameters (Γ_e, Γ_i) and a high-amplitude quenching effect is observed for interband scattering events leading to significant bandwidth broadening in imaginary conductivity. During the dominance of intraband scattering under low doping regime, we observed the emergence of new peak, which beats the universal conductivity for lower-frequency range of PB window in the real conductivity spectrum. The leap in response by excitonic effects in monolayer graphene is primarily triggered by dominant intraband scattering rather than interband scattering. It is very crucial that the material parameters of graphene such as carrier density, temperature, and impurity concentration, will dictate the importance of different scattering processes for transport dynamics.

ACKNOWLEDGMENTS

We gratefully acknowledge support from DST Science and Engineering Research Board (SERB), India under Grant No. SERB:CRG/2022/008749 and IIT Jodhpur Seed Grant No. I/SEED/BMK/20230017.

APPENDIX: KUBO EXPRESSIONS

In the following, we present some major steps for calculation of the conductivity. As long as the external field or the applied field perturbation is of the same order as the measured response, we are in the linear regime. From the CMBE, the first-order equation is deduced as follows,

$$\hbar\frac{\partial\rho^{(1)}_{n_1n_2k}(t)}{\partial t} = -i\big(\varepsilon_{n_1k}-\varepsilon_{n_2k}\big)\rho^{(1)}_{n_1n_2k}(t) - \Gamma^{(1)}_{n_1n_2}\rho^{(1)}_{n_1n_2k}(t) + ie\mathbf{E}(t).\big[\boldsymbol{\xi}_k,\rho^{(0)}_k\big]_{n_1n_2} - e\mathbf{E}(t).\nabla_k\rho^{(0)}_k, \quad \text{(A1)}$$

The solution in Eq. (10) is an initial guess where time derivative has only one time-dependent variable,

$$\frac{\partial\rho^{(1)}_{n_1n_2k}(t)}{\partial t} = -i\omega_1\rho^{(1)}_{n_1n_2k}(t). \quad \text{(A2)}$$

If Eq. (A2) is substituted in the first-order CMBE [Eq. (A1)], the expression becomes,

$$-i\hbar\omega_1\rho^{(1)}_{n_1n_2k}(t) = -i\hbar\omega_{n_1n_2k}\rho^{(1)}_{n_1n_2k}(t) - \Gamma^{(1)}_{n_1n_2}\rho^{(1)}_{n_1n_2k}(t) + ie\mathbf{E}(t).\big[\boldsymbol{\xi}_k,\rho^{(0)}_k\big]_{n_1n_2} - e\mathbf{E}(t).\nabla_k\rho^{(0)}_k, \quad \text{(A3)}$$

where the two-band frequency is actually the difference between any two bands ($\omega_{n_1n_2} = \omega_{n_1} - \omega_{n_2}$) and the phenomenological constant is actually dependent on the signs of n_1 and n_2. Eventually, from the Fourier transform of electric field one can find the final form with the density matrix.

$$\rho^{(1)}_{n_1n_2k}(t) = (-e)\int\frac{d\omega_1}{2\pi}E^c_{\omega_1}e^{-i\omega_1t} \times\frac{\big(\big[\xi^c_k,\rho^{(0)}_k\big]_{n_1n_2} + \frac{\partial}{\partial k_c}\rho^{(0)}_{n_1n_2k}\big)}{\hbar\omega_1 - \hbar\omega_{n_1n_2k} + i\Gamma^{(1)}_{n_1n_2}}. \quad \text{(A4)}$$

From the above expression of linear amplitude one can separate out the interband (first term) and intraband (second term) components. Then inverse transform of Eq. (A4) is substituted in Eq. (12) to get the first-order conductivity expression, which is a crucial step in matching the results of Kubo formalism. Formulated within the proximity of Dirac nodes (see Supplemental Material [34]) first the intraband expression is established using the energy terms as follows:

$\varepsilon_{1k} = +\hbar v_F k = \varepsilon$ and $\varepsilon_{2k} = -\hbar v_F k = -\varepsilon$. Similarly, the velocity terms are given by: $v^x_{11k} = +v_F k_x/k$ and $v^x_{22k} = -v_F k_x/k$. Eventually, the intraband linear conductivity expression can be written as,

$$\sigma^{(1)xx}_{\text{intra}}(\omega) = -e^2 \int \frac{d\mathbf{k}}{4\pi^2}\left[v^x_{11k}\mathcal{S}^{(1):x}_{11k}(\omega) + v^x_{22k}\mathcal{S}^{(1):x}_{22k}(\omega)\right]. \tag{A5}$$

The intraband frequency coefficient is now placed in the above expression along with the approximations taken around the Dirac point,

$$\sigma^{(1)xx}_{\text{intra}}(\omega) = -e^2 \int \frac{d\mathbf{k}}{4\pi^2}\left[\frac{iv^x_{11k}}{\hbar\omega + i\Gamma^{(1)}_i}\left(\frac{\partial f(\varepsilon)}{\partial\varepsilon}\frac{\partial\varepsilon}{\partial k_x}\right) + \frac{iv^x_{22k}}{\hbar\omega + i\Gamma^{(1)}_i}\left(\frac{\partial f(-\varepsilon)}{\partial\varepsilon}\frac{\partial\varepsilon}{\partial k_x}\right)\right], \tag{A6}$$

where $\rho^{(0)}_{n_1n_2k}$=$f(+\varepsilon)$ or f_{1k} is the Fermi-Dirac distribution function. If the intraband velocity matrix elements are substituted, the expression can be rewritten as,

$$\sigma^{(1)xx}_{\text{intra}}(\omega) = ie^2 \int \frac{d\mathbf{k}}{4\pi^2}\left(\frac{k_x}{k}\right)^2 \frac{v_F}{k} \times \frac{hv_F k}{\left(\hbar\omega + i\Gamma^{(1)}_i\right)}\left(\frac{\partial f(-\varepsilon)}{\partial\varepsilon} - \frac{\partial f(\varepsilon)}{\partial\varepsilon}\right). \tag{A7}$$

The transformation from momentum space to energy space is carried out to produce one half of the result obtained by Kubo expression,

$$\sigma^{(1)xx}_{\text{intra}}(\omega) = \frac{ie^2}{\pi\hbar\left(\hbar\omega + i\Gamma^{(1)}_i\right)} \int_0^\infty \varepsilon\left(\frac{\partial f(-\varepsilon)}{\partial\varepsilon} - \frac{\partial f(\varepsilon)}{\partial\varepsilon}\right)d\varepsilon. \tag{A8}$$

Above conversion can also be carried out using an identity, which is only applicable for two-dimensional isotropic materials given by,

$$\int \frac{d\mathbf{k}}{4\pi^2}\left(\frac{k_x}{k}\right)^2 \frac{v_F}{k} = \int \frac{d\mathbf{k}}{4\pi^2}\left(\frac{k_y}{k}\right)^2 \frac{v_F}{k} = \frac{1}{\pi\hbar}\int_0^\infty d\varepsilon. \tag{A9}$$

The proposition of the cold semiconductor approximation is put forward with the aim of attaining outcomes that closely converge towards temperatures nearing absolute zero. Similarly, for the interband term the required velocity approximations are listed $v^x_{12k} = iv_F k_y/k$ and $v^x_{21k} = -iv_F k_y/k$ along with the Berry connection elements $\xi^x_{12k} = k_y/2k^2$ and $\xi^x_{21k} = k_y/2k^2$. From Eq. (12) the interband linear conductivity expression is written as,

$$\sigma^{(1)xx}_{\text{inter}}(\omega) = -e^2 \int \frac{d\mathbf{k}}{4\pi^2}\left[v^x_{12k}\mathcal{S}^{(1):x}_{12k}(\omega) + v^x_{21k}\mathcal{S}^{(1):x}_{21k}(\omega)\right]. \tag{A10}$$

The interband frequency coefficient values are now placed in the above expression to become,

$$\sigma^{(1)xx}_{\text{inter}}(\omega) = -e^2 \int \frac{d\mathbf{k}}{4\pi^2}\left[\frac{-v^x_{12k}\xi^x_{12k}(f_{1k} - f_{2k})}{\left(\hbar\omega + i\Gamma^{(1)}_e - 2\varepsilon\right)} + \frac{v^x_{21k}\xi^x_{21k}(f_{1k} - f_{2k})}{\left(\hbar\omega + i\Gamma^{(1)}_e + 2\varepsilon\right)}\right]. \tag{A11}$$

If the interband velocity matrix elements are substituted in the numerator with some simple steps the expression can be rewritten as,

$$\sigma^{(1)xx}_{\text{inter}}(\omega) = \frac{ie^2}{2} \int \frac{d\mathbf{k}}{4\pi^2}\left(\frac{k_y}{k}\right)^2 \frac{v_F}{k}[f(+\varepsilon) - f(-\varepsilon)] \times \left[\frac{1}{\left(\hbar\omega + i\Gamma^{(1)}_e - 2\varepsilon\right)} + \frac{1}{\left(\hbar\omega + i\Gamma^{(1)}_e + 2\varepsilon\right)}\right]. \tag{A12}$$

Again, the transformation from momentum space to energy space is carried out to produce the other half of the result obtained by Kubo expression,

$$\sigma^{(1)xx}_{\text{inter}}(\omega) = \frac{ie^2}{\hbar\pi} \int_0^\infty \frac{d\varepsilon}{2}[f(+\varepsilon) - f(-\varepsilon)] \times \left[\frac{1}{\left(\hbar\omega + i\Gamma^{(1)}_e - 2\varepsilon\right)} + \frac{1}{\left(\hbar\omega + i\Gamma^{(1)}_e + 2\varepsilon\right)}\right]. \tag{A13}$$

Equivalence between the solution obtained and the expression without accounting for any scattering phenomena [20] can be formally demonstrated through some easy mathematical steps. Another important criteria that needs to be considered during vanishing of the interband phenomenological constant towards the positive side otherwise the entire has to be taken in the reverse order, which is not the target of our study. Furthermore, it should be noted that all the calculations hold true in the vicinity of absolute zero Kelvin. However, if necessary, appropriate adjustments to the chemical potential can be made to accommodate variations outside this temperature range. The indirect dependence of the scattering constant on temperature can be elucidated by expressing it in terms of curve fitting. Employing this approach, a more lucid comprehension of the thermal effects is attained, enabling the observation of temperature-related patterns and behaviors in the scattering constant.

[1] M. I. Katsnelson, Optics and response functions, *The Physics of Graphene*, 2nd ed. (Cambridge University Press, Cambridge, 2020), p. 168.

[2] A. Agrawal and G.-C. Yi, Photonic and optoelectronic applications of graphene: nonlinear optical properties of graphene and its applications, *Recent Advances in Graphene and Graphene-Based Technologies*, 2053–2563 (IOP Publishing, Bristol, 2023), pp. 9-1–9-22.

[3] P. Rickhaus, R. Maurand, M.-H. Liu, M. Weiss, K. Richter, and C. Schönenberger, Ballistic interferences in suspended graphene, Nat. Commun. **4**, 2342 (2013).

[4] X. Du, I. Skachko, A. Barker, and E. Y. Andrei, Approaching ballistic transport in suspended graphene, Nature Nanotechnol. **3**, 491 (2008).
[5] A. S. Mayorov, R. V. Gorbachev, S. V. Morozov, L. Britnell, R. Jalil, L. A. Ponomarenko, P. Blake, K. S. Novoselov, K. Watanabe, T. Taniguchi, and A. K. Geim, Micrometer-scale ballistic transport in encapsulated graphene at room temperature, Nano Lett. **11**, 2396 (2011).
[6] P. Y. Yu and M. Cardona, *Fundamentals of Semiconductors: Physics and Materials Properties*, Advanced Texts in Physics Vol. 3 (Springer, Berlin, 2005).
[7] K. S. Novoselov, A. K. Geim, S. V. Morozov, D. Jiang, M. I. Katsnelson, I. V. Grigorieva, S. V. Dubonos, and A. A. Firsov, Two-dimensional gas of massless Dirac fermions in graphene, Nature (London) **438**, 197 (2005).
[8] C.-H. Park, L. Yang, Y.-W. Son, M. L. Cohen, and S. G. Louie, New generation of massless Dirac fermions in graphene under external periodic potentials, Phys. Rev. Lett. **101**, 126804 (2008).
[9] S. Das Sarma, S. Adam, E. H. Hwang, and E. Rossi, Electronic transport in two-dimensional graphene, Rev. Mod. Phys. **83**, 407 (2011).
[10] A. H. Castro Neto, F. Guinea, N. M. R. Peres, K. S. Novoselov, and A. K. Geim, The electronic properties of graphene, Rev. Mod. Phys. **81**, 109 (2009).
[11] P. R. Wallace, The band theory of graphite, Phys. Rev. **71**, 622 (1947).
[12] E. Suárez Morell, J. D. Correa, P. Vargas, M. Pacheco, and Z. Barticevic, Flat bands in slightly twisted bilayer graphene: Tight-binding calculations, Phys. Rev. B **82**, 121407(R) (2010).
[13] T. Stauber, T. Low, and G. Gómez-Santos, Linear response of twisted bilayer graphene: Continuum versus tight-binding models, Phys. Rev. B **98**, 195414 (2018).
[14] L. A. Falkovsky and A. A. Varlamov, Space-time dispersion of graphene conductivity, Eur. Phys. J. B **56**, 281 (2007).
[15] V. P. Gusynin and S. G. Sharapov, Transport of Dirac quasiparticles in graphene: Hall and optical conductivities, Phys. Rev. B **73**, 245411 (2006).
[16] K. Ziegler, Robust transport properties in graphene, Phys. Rev. Lett. **97**, 266802 (2006).
[17] G. D. Mahan, *Many Particle Physics, Third Edition* (Plenum, New York, 2000).
[18] D. Ferry, *An Introduction to Quantum Transport in Semiconductors* (Jenny Stanford Publishing, Singapore, 2017).
[19] J. L. Cheng, N. Vermeulen, and J. E. Sipe, Third-order nonlinearity of graphene: Effects of phenomenological relaxation and finite temperature, Phys. Rev. B **91**, 235320 (2015).
[20] J. L. Cheng, N. Vermeulen, and J. E. Sipe, Third order optical nonlinearity of graphene, New J. Phys. **16**, 053014 (2014).
[21] J. L. Cheng, N. Vermeulen, and J. E. Sipe, Dc current induced second order optical nonlinearity in graphene, Opt. Express **22**, 15868 (2014).
[22] F. Hipolito, A. Taghizadeh, and T. G. Pedersen, Nonlinear optical response of doped monolayer and bilayer graphene: Length gauge tight-binding model, Phys. Rev. B **98**, 205420 (2018).
[23] J. L. Cheng, J. E. Sipe, S. W. Wu, and C. Guo, Intraband divergences in third order optical response of 2D systems, APL Photon. **4**, 034201 (2019).
[24] I. Al-Naib, J. E. Sipe, and M. M. Dignam, High harmonic generation in graphene at terahertz frequencies, in *CLEO: 2014* (Optica Publishing Group, Washington, DC, 2014), p. FTh1C.5.
[25] R. McGouran and M. M. Dignam, Nonlinear response of biased bilayer graphene at terahertz frequencies, Phys. Rev. B **96**, 045439 (2017).
[26] R. Anvari, E. Zaremba, and M. M. Dignam, Impact of nitrogen doping on the linear and nonlinear terahertz response of graphene, Phys. Rev. B **104**, 155402 (2021).
[27] J. L. Cheng and C. Guo, Nonlinear magneto-optic effects in doped graphene and in gapped graphene: A perturbative treatment, Phys. Rev. B **97**, 125417 (2018).
[28] G. B. Ventura, D. J. Passos, J. M. B. Lopes dos Santos, J. M. Viana Parente Lopes, and N. M. R. Peres, Gauge covariances and nonlinear optical responses, Phys. Rev. B **96**, 035431 (2017).
[29] J. E. Sipe and E. Ghahramani, Nonlinear optical response of semiconductors in the independent-particle approximation, Phys. Rev. B **48**, 11705 (1993).
[30] C. Aversa and J. E. Sipe, Nonlinear optical susceptibilities of semiconductors: Results with a length-gauge analysis, Phys. Rev. B **52**, 14636 (1995).
[31] L. M. Malard, K. F. Mak, A. H. C. Neto, N. M. R. Peres, and T. F. Heinz, Observation of intra- and inter-band transitions in the transient optical response of graphene, New J. Phys. **15**, 015009 (2013).
[32] T. Gu, N. Petrone, J. F. McMillan, A. van der Zande, M. Yu, G. Q. Lo, D. L. Kwong, J. Hone, and C. W. Wong, Regenerative oscillation and four-wave mixing in graphene optoelectronics, in *2012 Conference on Lasers and Electro-Optics (CLEO)* (IEEE, Piscataway, NJ, 2012), pp. 1–2.
[33] Z. Q. Li, E. A. Henriksen, Z. Jiang, Z. Hao, M. C. Martin, P. Kim, H. L. Stormer, and D. N. Basov, Dirac charge dynamics in graphene by infrared spectroscopy, Nature Phys. **4**, 532 (2008).
[34] See Supplemental Material at http://link.aps.org/supplemental/10.1103/PhysRevB.109.125428 for derivation of important approximations, taken around Dirac point.